Effects of nuclear deformation on fusion probability in the reactions of ^{82}Se+ ^{nat}Ce and ^{76}Ge+^{150}Nd near the Coulomb barrier

K. Nishio,[1] H. Ikezoe,[1] S. Mitsuoka,[1] K. Satou,[1] and S. C. Jeong[2]
[1]*Advanced Science Research Center, Japan Atomic Energy Research Institute, Tokai-mura, Ibaraki 319-1195, Japan*
[2]*Institute of Particle and Nuclear Studies, KEK, Tsukuba, Ibaraki 305-0801, Japan*
(Received 18 July 2000; published 23 March 2001)

Evaporation residue (ER) cross sections for ^{82}Se+^{nat}Ce ($Z_1Z_2=1972$) were measured in the vicinity of the Coulomb barrier and the fusion probability was obtained with the aid of calculated survival probability. This fusion probability was compared with that for ^{76}Ge+^{150}Nd ($Z_1Z_2=1920$), which was determined with the same manner by using the data published by us. The former system represents fusion of two spherical nuclei, the latter fusion involving the prolately deformed target ^{150}Nd. The collision of ^{76}Ge with the side of ^{150}Nd is the most compact configuration at touching. The system ^{82}Se+^{nat}Ce showed fusion hindrance in the form of extra-extra-push energy of 27 ± 5 MeV, whereas the system ^{76}Ge+^{150}Nd does not show fusion hindrance at and above the Coulomb barrier energy, suggesting that the reaction starting from the compact touching point results in a higher fusion probability.

DOI: 10.1103/PhysRevC.63.044610 PACS number(s): 25.60.Pj, 24.60.Dr

I. INTRODUCTION

Heavy ion fusion reactions between massive nuclei near the Coulomb barrier have been investigated experimentally and theoretically so far. This is partly because there is a possibility of synthesizing a super-heavy element as an evaporation residue by complete fusion under a proper choice of colliding particles and the bombarding energy. The production of evaporation residues is comprised of two separate processes: the fusion process between two interacting nuclei (entrance channel) and the survival process against fission in the course of the deexcitation process (exit channel). The former process is successfully understood by a coupled channel model [1] in the limit of light projectile-target combination of $Z_1Z_2\leqslant1800$. Fusion enhancement relative to the one-dimensional barrier penetration model was observed below the Coulomb barrier region [2]. This could be explained by replacing the one-dimensional barriers by a distribution of barriers [3–5]. The origins of the barrier distribution are the nuclear deformation, the inelastic couplings of the vibrational states in the colliding nuclei, and the nuclear transfer couplings. On the other hand, in heavy systems ($Z_1Z_2>1800$), the formation of a compound nucleus is not warranted even if the system overcomes the fusion barrier. This is because at the contact point the distance between the centers of projectile and target is larger than the distance of the centers of the nascent fission fragments at the fission saddle point. The kinetic energy of the interacting nuclei decreases in the course of the fusion process, with the energy being dissipated into the intrinsic excitation energy, and the system fails to surmount the fission saddle point for the bombarding energy corresponding to the Coulomb barrier. To drive the system into the compound nucleus, an additional energy called extra-extra-push energy (E_{XX}) is needed.

Collisions that fail to form a compound nucleus may break as quasifission after a significant amount of nucleon transfer and kinetic energy loss. Fission fragments from quasifission are difficult to distinguish experimentally from fission fragments of complete fusion, making the fusion cross section ambiguous when only the fission fragments are measured. Therefore detecting the evaporation residues is essential to identify the fusion reaction and obtain the fusion probability.

There are several investigations on the fusion hindrance of massive system based on the measurement of evaporation residues [5–8]. These investigations show that E_{XX} increases with Z_1Z_2 above $Z_1Z_2\sim1800$.

Recently, we investigated the fusion involving a deformed target nucleus and discussed the fusion hindrance from the measurement of evaporation residue cross sections [9,10]. In the ^{76}Ge+^{150}Nd [10] system ($Z_1Z_2=1920$), there is a fusion hindrance at the energy corresponding to the collision of ^{76}Ge with the tip of the prolately deformed ^{150}Nd ($\beta_2=0.358$ $\beta_4=0.104$ [11,12]), and an extra-extra-push energy of 13 MeV was determined (fusion barrier height in the tip collision is 184 MeV, determined by the CCDEF code [13]). On the other hand, there was no fusion hindrance for the side collision of $\theta_{coll}>50°$, where the barrier height is nearly constant within 211–215 MeV and is close to the Coulomb barrier $V_B=209$ MeV (see Fig. 10 in Ref. [10]). Note that V_B is calculated from the CCDEF code by assuming the interacting nuclei to be spherical and is referred to as spherical Coulomb barrier hereafter. We expected that the ^{76}Ge $+^{150}$Nd system exhibits larger fusion probability than the system consisting of spherical colliding nuclei whose Z_1Z_2 value is close to that of ^{76}Ge+ ^{150}Nd. In order to test this supposition, we chose the fusion reaction ^{82}Se $+^{nat}$Ce ($Z_1Z_2=1972$), leading to compound nuclei ^{222,224}U which are similar to ^{226}U from ^{76}Ge+^{150}Nd, and the ER cross sections were measured. From the experimental data we obtained the fusion probability of ^{82}Se+^{nat}Ce with the help of statistical model calculations which derives the survival probability. The result was compared with the fusion probability of ^{76}Ge+^{150}Nd, obtained in the same manner using the data published previously by us, in order to find the difference in the fusion probability between two types of

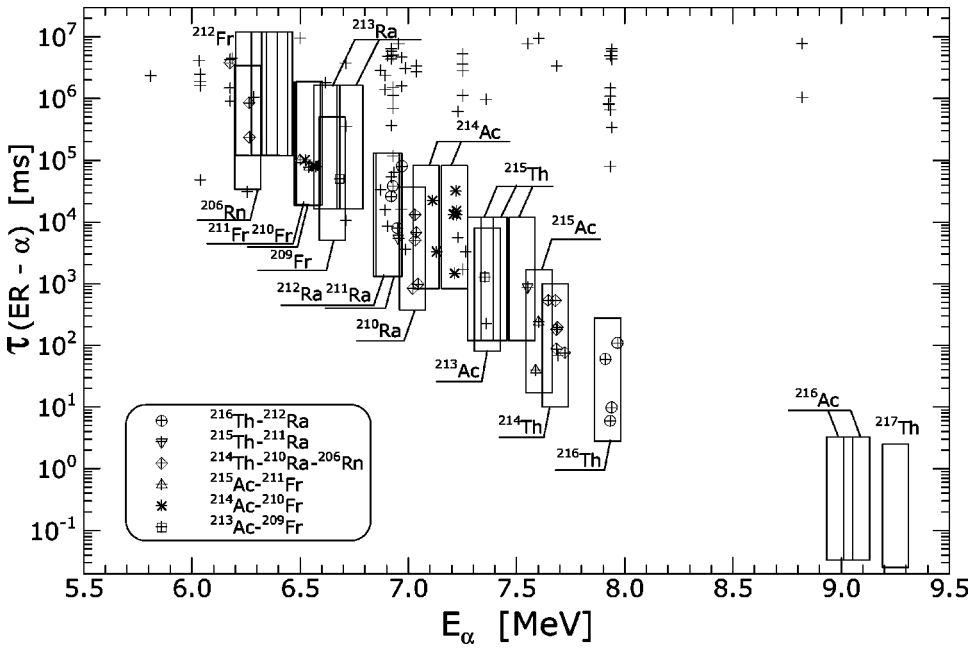

FIG. 1. Events of ER-α correlation plotted on the plane of α energy (E_α) and time interval (τ) for ^{82}Se+$^{\text{nat}}$Ce. τ is limited to 10 000 s in this spectrum. The corresponding center-of-mass energy is 245.0 MeV. Each box represents α decay character having ± 60 keV energy width around the known α line and time interval of $\frac{1}{10}T_{1/2} < \tau < 10T_{1/2}$. Correlated chain ER-$\alpha_1$-$\alpha_2$ is shown depending on the channel. For the channel starting from ^{214}Th, the decay chain up to α_3 is observed.

fusion reactions: the one using spherical nuclei and the other involving largely deformed nuclei.

II. EXPERIMENT

Measurement of evaporation residue cross sections following the fusion of ^{82}Se+$^{\text{nat}}$Ce was made by using ^{82}Se beam supplied by the JAERI-tandem booster accelerator. The targets were made by sputtering the natural cerium metal (abundance of ^{140}Ce and ^{142}Ce are 88.5 and 11.1%, respectively) on a 1.5 μm thick aluminum foil, and the thickness was 425 μg/cm^2. The $^{\text{nat}}$Ce target was set to a rotating target frame in the target chamber.

Since the evaporation residues produced in the present reaction are α decaying nuclei, the evaporation channels could be identified by observing α-decay energies and lifetimes. The experimental details are described elsewhere [9,10], and thus only the essence is written here. The evaporation residues emitted in beam direction were separated in flight from the primary beam by the JAERI recoil mass separater (JAERI-RMS) [14]. The separated recoils were implanted into a double sided position-sensitive strip detector (DPSD). Two large area timing detectors, one positioned in front of the DPSD and the other 30 cm upstream the DPSD, were used to obtain the time-of-flight (TOF) signal of incoming particles. The presence of the TOF signal was used to distinguish ER implantation events from the subsequent α decays, which generate no TOF signals. A two-dimensional spectrum of the energy versus TOF gave a rough estimate of a mass number of the incoming particle, allowing the distinction of ERs from background particles. Alpha-decay events later than 5 μs after the implantation of ER were recorded. The energy calibration of the DPSD was made using known α transition energy from ^{216}Th(7.921 MeV) [15] which were produced in the present reactions. Typical energy resolution of the DPSD was 70 keV(FWHM). A silicon surface barrier detector to monitor the beams was set at 45° direction in the target chamber to determine the absolute values of the ER cross sections.

III. DATA ANALYSIS AND EXPERIMENTAL RESULT

The identification for a specific channel was made by counting the ER-α_1-α_2 chains, where ER stands for the events produced when the incoming evaporation residue hits the DPSD. The α_1 and α_2 are the first and the second correlated α-decay event. Figure 1 shows the two-dimensional spectrum of α particle energy and the time interval between the ER implantation and the α decay. All the events shown in Fig. 1 satisfy the condition that the position difference between ER and α event has to be less than $(\Delta X, \Delta Y) = (1.0, 1.0)$ mm. We searched the correlated decay chain, ER-α_1-α_2, to identify the specific evaporation channels with help of the known α decay energy and half-life. The events forming ER-α_1-α_2 chains are shown in Fig. 1, where each channel is distinguished by different symbols. Since the α-decay energies and half-lives of ^{215}Th and ^{213}Ac are almost similar, we obtained the cross section in the form of ^{215}Th+ ^{213}Ac. Also if α_1 escaped the detector with the energy deposition larger than the discrimination energy (2 MeV) of the DPSD, the identification was possible when the full energy of α_2 was detected except the chain including ^{216}Ac(α_1), for which the corresponding daughter ^{212}Fr(α_2) has a long half-life of 20.0 min and consequently the identification was impossible due to chance coincidences. The ^{211,212}Ra box contains 11 events, which is significantly larger than the five events arising from ER-^{216}Th-^{212}Ra and ER-^{215}Th-^{211}Ra chains. This difference is attributed to the direct production of ^{211,212}Ra as evaporation residue.

To obtain absolute ER cross sections the efficiency of the ER to be transported to the focal plane detectors through the JAERI-RMS has to be known, which was estimated by the method described in Refs. [10,16]. The estimated transport efficiency for a specific charge state of ER was multiplied by

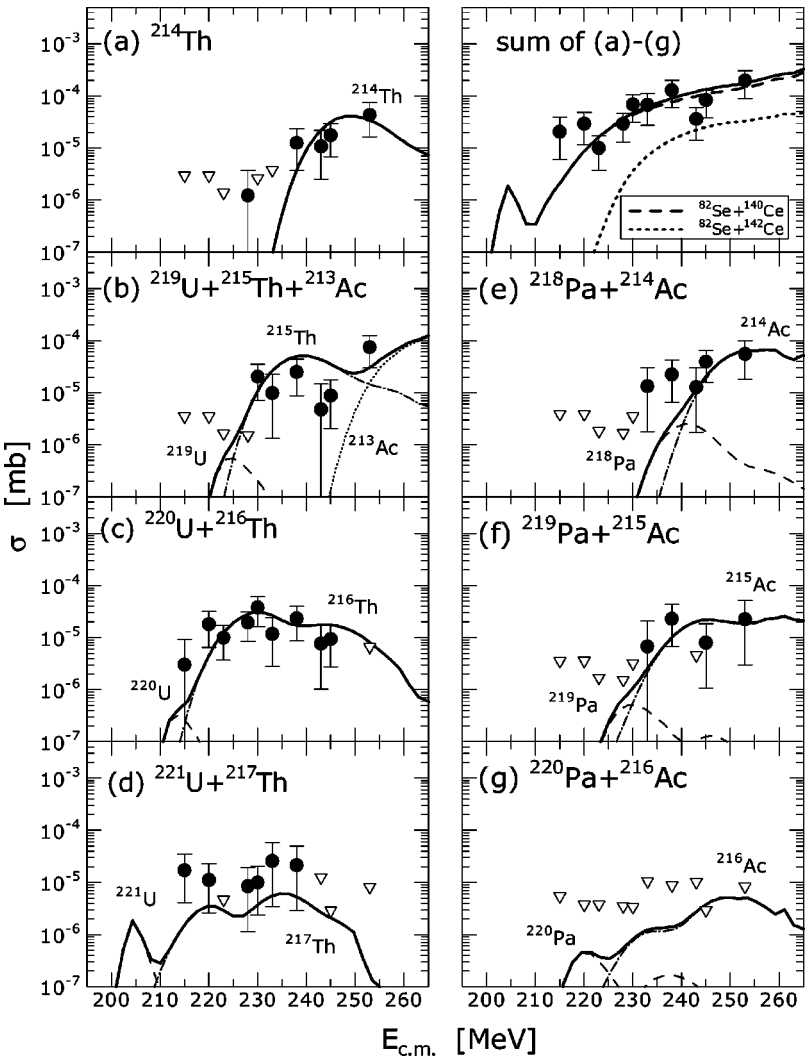

FIG. 2. Evaporation residue cross sections for ^{82}Se+ ^{nat}Ce are shown by solid circles in (a)–(g). The upper right section is the sum of the cross sections over the channels (a)–(g). Reversed triangle is the upper limit defined by the cross section of one event detection. Thick solid curve in each section is the result of the statistical model calculation (HIVAP code) in which the fusion probability determined by Eqs. (2)–(4) with $(E_{XX},\sigma_B)=(27,10)$ MeV is adopted in the entrance channel. The cross section of (b)–(g) includes the components noted in each figure and the corresponding cross sections calculated are shown by the thin curves (dashed: ^{219,220,221}U and ^{218,219,220}Pa, dash-dotted: ^{215,216,217}Th and ^{214,215,216}Ac, dotted: ^{213}Ac). In the section of the sum spectrum over (a)–(g) the cross sections arising from the ^{82}Se+ ^{140}Ce (thick dashed) and ^{82}Se+ ^{142}Ce (thick dotted) are shown.

the charge fraction calculated by the Shima formula [17]. The transport efficiency for the αxn channels ranged from 0.22 to 0.33 depending on the beam energy. The xn efficiency ranged from 0.29 to 0.40. The estimation does not show a significant difference between αxn and αpxn efficiencies.

The probability of detecting the α decay of evaporation residues implanted in the DPSD was taken into account in the analysis. This is the function of ER kinetic energy (thus the implantation depth) and the α decay energy. For example, the probability of full energy absorption of α particles from ^{217}Th was 0.62 at $E_{\mathrm{c.m.}}=238.0$ MeV. The escaped event of this α decay was detected with the probability 0.24 with respect to the present energy discrimination of 2 MeV. We also took into account the α decay branch in the α-EC(β^+) competition by referring to [15].

The obtained evaporation residue cross sections for ^{82}Se $+$ ^{nat}Ce are shown in Fig. 2 as a function of c.m. energy of ^{82}Se+ ^{140}Ce, which is determined in the middle of the target layer. The data are also listed in Table I. The error includes both statistical contributions and the estimated uncertainty of 50% coming from the transport efficiency of ERs through the JAERI-RMS. The cross section determined from the ER-^{216}Th-^{212}Ra chain in Fig. 2(c) may include the components of ^{220}U channel, which cannot be detected in this experiment because of the short half-life (unknown). This is the situation for the channels (b), (d)–(g). The upper right section of Fig. 2 represents the sum of ER cross sections over the channels of (a)–(g). Estimated upper limits of the cross section are shown by the symbol ∇ in Fig. 2 and also in Table I. Even though the isotope ^{142}Ce is the minor constituent in the ^{nat}Ce target (11.5%), the ER cross sections contain the component arising from the ^{82}Se+ ^{142}Ce reaction. This will be discussed in the next section on the basis of the statistical model calculation.

IV. DISCUSSIONS

The experimental ER cross section $\sigma_{\mathrm{er},c}$ for the observed channel c was used to obtain the fusion probability weighted by the angular momentum l by

$$P_{\mathrm{fus}}(E_{\mathrm{c.m.}})=\frac{\sum_c \sigma_{\mathrm{er},c}(E_{\mathrm{c.m.}})}{\pi\lambda^2\sum_l (2l+1)\sum_c w_{\mathrm{er},c}(E_{\mathrm{c.m.}}+Q,l)}. \quad (1)$$

TABLE I. Summary of evaporation residue cross sections in [nb] from the reaction of ^{82}Se+ ^{nat}Ce for the channels of (a) ^{214}Th, (b) ^{219}U+ ^{215}Th+ ^{213}Ac, (c) ^{220}U+ ^{216}Th, (d) ^{221}U+ ^{217}Th, (e) ^{218}Pa+ ^{214}Ac, (f) ^{219}Pa+ ^{215}Ac, and (g) ^{220}Pa+ ^{216}Ac. Upper limit is shown in parentheses when no event is detected. The last column shows the sum of ER cross sections over (a)–(g).

$E_{c.m.}$	(a)	(b)	(c)	(d)	(e)	(f)	(g)	sum
215.0	(3.0)	(3.5)	$3.0^{+6.2}$	$17.3^{+18.0}_{-13.2}$	(3.9)	(3.6)	(5.4)	$20.3^{+18.3}_{-14.4}$
220.0	(3.0)	(3.5)	$18.1^{+13.8}_{-11.7}$	$11.2^{+11.6}_{-8.5}$	(3.9)	(3.6)	(3.8)	$29.3^{+19.6}_{-17.6}$
223.0	(1.4)	(1.7)	$10.0^{+7.2}_{-6.2}$	(4.7)	(1.8)	(1.7)	(3.8)	$10.0^{+7.2}_{-6.3}$
228.0	$1.2^{+2.5}$	(1.5)	$19.5^{+11.6}_{-11.0}$	$8.4^{+11.0}_{-7.3}$	(1.7)	(1.5)	(3.5)	$29.2^{+16.9}_{-16.1}$
230.0	(2.6)	$20.2^{+15.4}_{-13.1}$	$38.0^{+23.0}_{-21.6}$	$10.0^{+10.4}_{-7.7}$	(3.2)	(3.3)	(3.4)	$68.3^{+38.2}_{-37.0}$
233.0	(3.8)	$9.8^{+12.9}_{-8.5}$	$11.8^{+12.3}_{-9.1}$	$25.6^{+33.5}_{-22.2}$	$13.3^{+17.4}_{-11.5}$	$6.8^{+14.0}$	(10.6)	$67.5^{+43.9}_{-39.9}$
238.0	$12.5^{+11.3}_{-8.8}$	$24.8^{+18.9}_{-16.0}$	$23.3^{+16.8}_{-14.6}$	$21.6^{+28.2}_{-18.7}$	$22.4^{+20.2}_{-15.8}$	$22.8^{+20.6}_{-16.1}$	(8.9)	127^{+70}_{-68}
243.0	$10.7^{+11.2}_{-8.2}$	$4.8^{+9.9}$	$7.7^{+10.0}_{-6.6}$	(12.5)	$12.8^{+16.8}_{-11.1}$	(4.6)	(10.3)	$36.0^{+24.9}_{-22.1}$
245.0	$17.5^{+12.1}_{-10.7}$	$8.8^{+9.1}_{-6.7}$	$9.4^{+8.4}_{-6.6}$	(2.9)	$39.3^{+25.5}_{-23.3}$	$8.0^{+10.5}_{-6.9}$	(2.9)	$83.0^{+45.7}_{-44.5}$
253.0	$43.2^{+31.2}_{-27.1}$	$74.2^{+49.6}_{-44.6}$	(6.6)	(8.2)	$55.3^{+45.2}_{-37.1}$	$22.5^{+29.4}_{-19.5}$	(8.3)	195^{+109}_{-106}

The survival probability $w_{er,c}$ against fission for the specific evaporation channel c is a function of the excitation energy $E_{ex}=E_{c.m.}+Q$ (reaction Q value) and the angular momentum l. This was calculated by the HIVAP code [18] using the parameters described in Refs. [9,10] except the slight modification of the scaling factor of the fission barrier height. To check if the present statistical model calculation reasonably provides the survival probability, we have determined the P_{fus} for the fusion reaction ^{28}Si+ ^{198}Pt by using the data in Ref. [10], which is the light fusion system with $Z_1Z_2=1092$ and is expected to have no fusion hindrance. The result is shown in Fig. 3 as a function of $E_{c.m.}/V_B$, where $V_B=125.5$ MeV is the spherical Coulomb barrier for this reaction. Above this barrier P_{fus} is almost constant with 1, indicating that the present HIVAP calculation reasonably reproduces the survival probability. We want to mention that P_{fus} at the two lowest energies have large values of 0.2 -0.3 even below the spherical Coulomb barrier. This indicates the fusion enhancement primarily due to the deformation of ^{28}Si [10].

When fission is the dominant deexcitation channel like in the present case, the evaporation residue cross section does not contain information on the fusion of high partial waves, because they will lead to fission. The surviving l range is limited to $l<\sim 25\hbar$, corresponding to an impact parameter less than 1 fm, and hence P_{fus} is reasonably approximated to that of central collision.

The fusion probability for ^{82}Se+ ^{nat}Ce was determined from the ER cross sections with the assumption that the P_{fus} for ^{82}Se+ ^{140}Ce and ^{82}Se+ ^{142}Ce are the same. This assumption is justified by the weak dependence of E_{XX} on the target isotopes investigated for the fusion of ^{86}Kr + ^{121,123}Sb ($Z_1Z_2=1836$) and ^{124}Sn+ ^{90,92,94,96}Zr ($Z_1Z_2=2000$) [7]. The difference of two neutrons in the target (Sb or Zr) changes the E_{XX} value only less than 4 MeV (error of $3-5$ MeV is reported in E_{XX}). The surviving probability of a specific channel, $w_{er,c}$ [see Eq. (1)], includes two components representing the decay of compound nuclei ^{222}U (^{82}Se+ ^{140}Ce) and ^{224}U (^{82}Se+ ^{142}Ce) with their fraction being determined in accordance with isotope abundance. The obtained fusion probability for ^{82}Se+ ^{nat}Ce is shown in Fig. 3 as a function of $E_{c.m.}/V_B$, where V_B is taken as 215.3 MeV of ^{82}Se+ ^{140}Ce. The error in P_{fus} includes only statis-

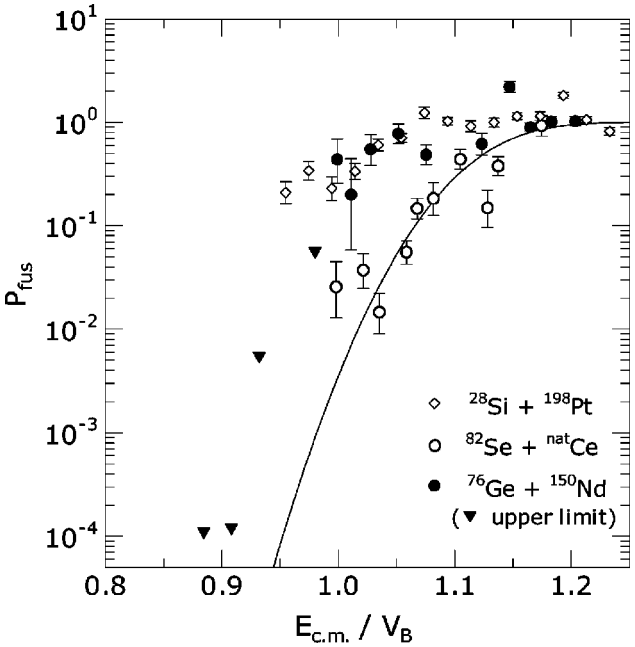

FIG. 3. Fusion probability P_{fus} for ^{28}Si+ ^{198}Pt (open diamond), ^{82}Se+ ^{nat}Ce (open circle), and ^{76}Ge+ ^{150}Nd (solid circle) determined from the experimental ER cross sections. Reversed triangle (solid) is the upper limit for ^{76}Ge+ ^{150}Nd. Solid curve is the fusion probability of ^{82}Se+ ^{nat}Ce calculated by Eqs. (2)–(4). Details are described in the text.

tical error. Below $E_{\mathrm{c.m.}}/V_B=1.15$, P_{fus} for ^{82}Se+$^{\mathrm{nat}}$Ce decreases considerably with lowering the bombarding energy, exhibiting the curve similar to the massive system having fusion hindrance [5,7,8]. By finding the $E_{\mathrm{c.m.}}$ at which P_{fus} of ^{82}Se+$^{\mathrm{nat}}$Ce crosses the $P_{\mathrm{fus}}=0.5$ level, we obtained the extra-extra-push energy $E_{XX}=27\pm5$ MeV for this reaction.

The authors of Refs. [7,8] investigated the fusion probability for the massive and nearly symmetric fusion reactions and found that the fusion probability is reproduced by assuming the fusion barrier distribution f_B to have Gaussian shape of a mean value $E_B=V_B+E_{XX}$ and a standard deviation σ_B,

$$P_{\mathrm{fus}}(E_{\mathrm{c.m.}})=\int_{E_{\min}}^{E_{\max}} dE'_B f_B(E'_B;E_B,\sigma_B)T_{l=0}(E_{\mathrm{c.m.}},E'_B), \tag{2}$$

$$f_B(E'_B;E_B,\sigma_B)=\frac{1}{\sqrt{2\pi}\sigma_B}\exp\{-(E'_B-E_B)^2/2\sigma_B^2\}, \tag{3}$$

$$T_{l=0}(E_{\mathrm{c.m.}},E'_B)=\left[1+\exp\left\{\frac{2\pi}{\hbar\omega}(E'_B-E_{\mathrm{c.m.}})\right\}\right]^{-1}. \tag{4}$$

Equation (4) is the *s*-wave transmission probability ($l=0$) of the barrier E'_B and ignores the centrifugal potential (V_l), from the consideration that V_l is only about 1.0 MeV at $l=20\hbar$. The barrier curvature $\hbar\omega$ is taken as 2.92 MeV for ^{82}Se+^{140}Ce from the CCDEF code [13]. The integration range ($E_{\min}$,$E_{\max}$) was set ($E_B-10\sigma_B$, $E_B+10\sigma_B$) in this study. We found that P_{fus} for ^{82}Se+$^{\mathrm{nat}}$Ce agrees reasonably with the expressions (2)–(4) by taking (E_{XX},σ_B) =(27, 10) MeV, as shown by the solid curve in Fig. 3. It must be noted here that σ_B has a rather large uncertainty of about 2 MeV.

We compared the present E_{XX} value of ^{82}Se+$^{\mathrm{nat}}$Ce with the prediction of Quint systematics [8] by standing on his scaling parameter $Z_1Z_2+10\nu_{\min}$, where $\nu_{\min}$ is determined by the number of particles or holes of projectile and target, and represents the structure effects on the fusion process. For ^{82}Se+^{140}Ce ($\nu_{\min}=2$), the Quint systematics predicts $E_{XX}=\sim21$ MeV, which is close to the present value.

By assuming Gaussian barrier distribution f_B of (E_{XX},σ_B)=(27, 10) MeV for ^{82}Se+$^{\mathrm{nat}}$Ce and the barrier penetrability of the Hill-Wheeler formula [Eq. (4)] including the centrifugal potential, we constructed the partial wave cross section $\sigma_l(E_{\mathrm{c.m.}})$ as $\pi\lambda\!\!\!^{-2}(2l+1)P_{\mathrm{fus}}(E_{\mathrm{c.m.}})$. This was inputted to the HIVAP code as an initial spin distribution and the ER cross sections were calculated. The calculated result is shown by the thick solid curves in Fig. 2. To obtain the ER cross sections for ^{82}Se+$^{\mathrm{nat}}$Ce, those for ^{82}Se+^{140}Ce and ^{82}Se+^{142}Ce were calculated and summed, considering the isotope abundances. It is found in Fig. 2 that the calculated cross sections agree with the experimental data in the channels (a)–(f). In the channel (g), the calculation lies below the upper limit and is consistent with the experiment. In the sum spectrum over the channels (a)–(g), two constituents coming from the fusion reaction, ^{82}Se+^{140}Ce and ^{82}Se+^{142}Ce, are shown, from which one can see the former component to be predominant in this spectrum.

The fusion probability P_{fus} for ^{76}Ge+^{150}Nd was determined by using our data [10] and the survival probability $w_{\mathrm{er},c}$ was calculated by the HIVAP code. The results are shown by the solid circles with statistical error bars in Fig. 3. P_{fus} values of ^{76}Ge+^{150}Nd is nearly flat with $\sim$1.0 down to $E_{\mathrm{c.m.}}\sim V_B$ ($V_B=209.0$ MeV). This trend is similar to the fusion of ^{28}Si+^{198}Pt which exhibits no fusion hindrance, and the spectrum shows marked contrast to that of ^{82}Se+$^{\mathrm{nat}}$Ce. It is apparent that the reaction ^{76}Ge+^{150}Nd has no fusion hindrance above the spherical Coulomb barrier. We did not observe any event in $E_{\mathrm{c.m.}}<V_B$ and thus the upper limit is shown by the solid reversed triangle in Fig. 3.

The anomalously large fusion probability for ^{76}Ge +^{150}Nd will be clear when one compares the present result with the prediction of the Quint systematics, $E_{XX}=25$ MeV, determined from the scaling $Z_1Z_2+10\nu_{\min}=2040$ for ^{76}Ge +^{150}Nd ($\nu_{\min}=12$).

Because of the strongly prolate shape of ^{150}Nd, the Coulomb barrier height depends on the colliding angle θ_{coll} of ^{76}Ge with the symmetry axis of ^{150}Nd. It was concluded in Ref. [10] that the collision of $\theta_{\mathrm{coll}}>50°$, which is the interaction of ^{76}Ge on the side of ^{150}Nd, results in a fusion without extra-extra-push energy, whereas the collision of ^{76}Ge with the tip results in quasifission. The side collision of $\theta_{\mathrm{coll}}>50°$ amounts to 65% in solid angle for ^{76}Ge+^{150}Nd system and the Coulomb barrier height at these angles is nearly constant with 210−215 MeV (see Fig. 10 in Ref. [10]) which is close to or slightly larger than the spherical Coulomb barrier.

The larger fusion probability of ^{76}Ge+^{150}Nd near the Coulomb barrier, compared with the fusion of ^{82}Se+$^{\mathrm{nat}}$Ce, may be related to the contact point of the interacting two nuclei relative to the fission saddle point of the compound nucleus, from the consideration that the necessary condition for forming a compound nucleus is the dynamical trajectory to pass inside the fission saddle point on the potential surface. The touching point of the fusing two nuclei is more compact in the configuration when ^{76}Ge collides with the side of ^{150}Nd than the fusion ^{82}Se+$^{\mathrm{nat}}$Ce. The side collision ($\theta=90°$) for ^{76}Ge+^{150}Nd gives a fusion barrier position of 11.7 fm, determined by using the CCDEF code, whereas the corresponding value of ^{82}Se+ ^{140}Ce becomes 12.3 fm. If we assume that the fission saddle points do not differ very much in the two systems (^{222}U for ^{82}Se+^{140}Ce and ^{226}U for ^{76}Ge+ ^{150}Nd), it can be considered that the configuration of side collision of ^{76}Ge+^{150}Nd is close to the fission saddle point, and thus the loss in kinetic energy in the fusion process is minimized in the side collision and is smaller than that for the fusion ^{82}Se+^{140}Ce. This discussion is supported by the theoretical consideration in Ref. [19], where they calculated the macroscopic potential energy surface of the interacting symmetric nuclei as well as the fission saddle point of the compound nucleus. For the light reaction system ($Z_1Z_2<1800$), the distance between the mass centers R_{sd} of the nascent fission fragments at the fission saddle point is

larger than the distance R_c between the mass centers of projectile and target at the contact point, so that the two colliding nuclei can fuse automatically after touching. On the other hand, for the heavy reaction systems ($Z_1Z_2>1800$), the distance R_{sd} is smaller than R_c, which means that an additional energy relative to the fusion barrier must be supplied in order to drive the dynamical trajectory inside the saddle point and form a compound nucleus.

The present result partly supports the theoretical consideration in the fusion reaction leading to a superheavy element, which is referred to as ''gentle fusion'' [20] or ''hugging fusion'' [21]. This type of fusion reaction suggests the possible enhancement of fusion probability when the projectile collides with a well deformed target nucleus with their symmetry axis being orthogonal. Since this is the most compact configuration at touching, the smallest distance between the saddle point and the interacting point is achieved. This specific configuration would presumably result in higher fusion probability than any other touching configuration.

V. SUMMARY

The evaporation residue cross sections for $^{82}Se+^{nat}Ce$ was measured in the vicinity of the Coulomb barrier, and the fusion probability for the central collision was determined. This is a reaction characterized by the spherical and massive colliding partners with $Z_1Z_2=1972$, and fusion hindrance was observed in the form of the extra-extra-push energy of 27 ± 5 MeV. We also determined the fusion probability of $^{76}Ge+^{150}Nd$, which has a Z_1Z_2 value of 1920. This is in striking contrast to the fusion probability of $^{82}Se+^{nat}Ce$ and does not exhibit any fusion hindrance above the spherical Coulomb barrier. The different fusion probabilities between two types fusion reaction suggest that the nuclear deformation plays an important role in the fusion process. The phenomenon that fusion is not hindered when ^{76}Ge collides with the side of the prolately deformed target ^{150}Nd, suggested in the current analysis as well as the previous work [10], supports that the reaction starting from the compact touching point results in higher fusion probability than the fusion from the distant touching point.

ACKNOWLEDGMENTS

The authors thank the crew of the JAERI tandem-booster facility for the beam operation. Special thanks are due to Dr. Takeishi for supplying us with the cerium sample. We thank Mr. Sakama of Tokyo Metropolitan University for his support on this experiment.

[1] A. B. Balantekin and N. Takigawa, Rev. Mod. Phys. **70**, 77 (1998).
[2] M. Dasgupta, D. J. Hinde, N. Rowley, and A. M. Stefani, Annu. Rev. Nucl. Part. Sci. **48**, 401 (1998).
[3] N. Rowley, G. R. Satchler, and P. H. Stelson, Phys. Lett. B **254**, 25 (1991).
[4] W. Reisdorf, F. P. Hessberger, K. D. Hildenbrand, S. Hofmann, G. Münzenberg, K.-H. Schmidt, J. H. R. Schneider, W. F. W. Schneider, K. Sümmerer, G. Wirth, J. V. Kratz, and K. Schlitt, Phys. Rev. Lett. **49**, 1811 (1982).
[5] J. G. Keller, K.-H. Schmidt, F. P. Hessberger, G. Münzenberg, W. Reisdorf, H.-G. Clerc, and C.-C. Sahm, Nucl. Phys. **A452**, 173 (1986).
[6] C.-C. Sahm, H.-G. Clerc, K.-H. Schmidt, W. Reisdorf, P. Armbruster, F. P. Hessberger, J. G. Keller, G. Münzenberg, and D. Vermeulen, Z. Phys. A **319**, 113 (1984).
[7] C.-C. Sahm, H.-G. Clerc, K.-H. Schmidt, W. Reisdorf, P. Armbruster, F. P. Hessberger, J. G. Keller, G. Münzenberg, and D. Vermeulen, Nucl. Phys. **A441**, 316 (1985).
[8] A. B. Quint, W. Reisdorf, K.-H. Schmidt, P. Armbruster, F. P. Hessberger, S. Hofmann, J. Keller, G. Münzenberg, H. Stelzer, H.-G. Clerc, W. Morawek, and C.-C. Sahm, Z. Phys. A **346**, 119 (1993).
[9] S. Mitsuoka, H. Ikezoe, K. Nishio, and J. Lu, Phys. Rev. C **62**, 054603 (2000).
[10] K. Nishio, H. Ikezoe, S. Mitsuoka, and J. Lu, Phys. Rev. C **62**, 014602 (2000).
[11] P. Raghavan, At. Data Nucl. Data Tables **42**, 189 (1989).
[12] P. Möller, J. R. Nix, W. D. Myers, and W. J. Swiatecki, At. Data Nucl. Data Tables **59**, 185 (1995).
[13] J. O. Fernández Niello, C. H. Dasso, and S. Landowne, Comput. Phys. Commun. **54**, 409 (1989).
[14] H. Ikezoe, Y. Nagame, T. Ikuta, S. Hamada, I. Nishinaka, and T. Ohtuki, Nucl. Instrum. Methods Phys. Res. A **376**, 420 (1996).
[15] R. B. Firestone, *Table of Isotopes*, edited by V. S. Shirley (Wiley, New York, 1996).
[16] T. Kuzumaki, H. Ikezoe, S. Mitsuoka, T. Ikuta, S. Hamada, Y. Nagame, I. Nishinaka, and O. Hashimoto, Nucl. Instrum. Methods Phys. Res. A **437**, 107 (1999).
[17] K. Shima, T. Ishihara, and T. Mikuno, Nucl. Instrum. Methods **200**, 605 (1982).
[18] W. Reisdorf and M. Schädel, Z. Phys. A **343**, 47 (1992).
[19] P. Möller and J. R. Nix, Nucl. Phys. **A272**, 502 (1976).
[20] W. Nörenberg, Proceedings of the International Workshop on Heavy-Ion Fusion, Padova, Italy, 1994.
[21] A. Iwamoto, P. Möller, J. R. Nix, and H. Sagawa, Nucl. Phys. **A596**, 329 (1996).